

A novel method for estimating sandbody compaction in fluvial successions

Wei Li ^{a,b}, Dali Yue ^{a,*}, Luca Colombera ^b, Nigel P. Mountney ^b, Shenghe Wu ^a

^a State Key Laboratory of Petroleum Resources and Prospecting, College of Geosciences, China University of Petroleum (Beijing), Beijing 102249, China

^b Fluvial & Eolian Research Group, School of Earth & Environment, University of Leeds, Leeds LS2 9JT, UK

ARTICLE INFO

Article history:

Received 21 March 2020

Received in revised form 21 April 2020

Accepted 22 April 2020

Available online 27 April 2020

Editor: Dr. Jasper Knight

Keywords:

Fluvial successions

Channel geometry

Channel bank

Angle of repose

Sediment compaction

Compactional porosity loss

ABSTRACT

Clastic sedimentary successions are subject to variable amounts of compaction, which causes a decrease in both the thickness and porosity of sand-rich depositional units. Methods for estimating the degree of sediment compaction are needed for characterizing changes in the geometry and petrophysical properties of depositional elements in relation to their burial history. Conventional methods for estimating compaction of rock successions through the application of several empirical equations return estimations whose uncertainties can be significant, and integrative approaches that can produce reliable estimations are therefore desirable. To this end, a new method is proposed here for the estimation of the degree of compaction of sandbodies in ancient channelized fluvial successions. For outcropping fluvial successions, the compacted geometry of channel-fill margins cut into non-cohesive deposits can be measured, whereas the decompact angle of repose of the material originally forming the channel banks can be estimated experimentally. Sediment compaction can therefore be estimated by comparing the observed geometry of the uppermost part of a channel-fill margin with the angle of repose of the non-cohesive bank material. The proposed method has been applied to three different sand-prone fluvial successions seen in outcrop, for the purposes of (i) illustrating the approach, and (ii) testing it through a comparison of its estimations against results produced by a conventional method based on thin-section observations. The comparison demonstrates that the two methods yield similar results, highlighting how the proposed approach can be readily applied to the assessment of compaction in clastic successions, for scopes of both pure and applied geological research.

© 2020 The Authors. Published by Elsevier B.V. This is an open access article under the CC BY-NC-ND license (<http://creativecommons.org/licenses/by-nc-nd/4.0/>).

1. Introduction

In ancient successions of clastic sedimentary rocks, sediment compaction causes the geometry and porosity of depositional elements to be reduced relative to those of equivalent sedimentary units from modern and recent systems (Perrier and Jacques, 1974). Depending on burial history and the maximum burial depth of a given sedimentary succession, sand-rich architectural elements such as channel bodies can be compacted to up to 70% of their original thickness, in some cases (Athy, 1930; Beard and Weyl, 1973; Ehrenberg, 1995). Hence, methods for estimating the degree of compaction of rock successions are needed to quantitatively characterize changes in the geometry and petrophysical properties of sand-prone sedimentary units.

Two methods are widely employed to estimate the compaction of subsurface clastic sedimentary successions: (i) compaction can be estimated based on the maximum burial depth using empirical

relationships relating the compaction ratio to burial depth, for known lithology types (e.g., Athy, 1930; Sreaton et al., 2002); and (ii) compaction ratios can otherwise be calculated based on thin-section observations as compactional porosity loss, by comparing the original (decompact) and current (or present) porosities after restoration of diagenetic effects (Perrier and Jacques, 1974; Sclater and Christie, 1980). Although widely used, both methods have shortcomings. For the first method, prior studies have demonstrated that the relationship between maximum burial depth and compaction ratio varies significantly, because compaction is affected by sediment composition, grain size, sorting, shape of particles, and by fluid pressure (e.g., Beard and Weyl, 1973; Sreaton et al., 2002; Ward et al., 2018). Moreover, the maximum burial depth cannot be readily determined in many cases, especially for outcropping successions. When estimating compaction through assessment of porosity loss according to the second method, uncertainty exists because the original porosities of sandstones can be highly variable depending on factors such as original grain sorting and packing (e.g., Beard and Weyl, 1973), which are themselves related to the original processes of sediment transport and deposition (Bridge and Lunt, 2006). As such, the original decompact porosity of ancient sandstones cannot necessarily be known confidently when applying

* Corresponding author.

E-mail addresses: wei_li_geologist@qq.com (W. Li), yuedali@cup.edu.cn (D. Yue), L.Colombera@leeds.ac.uk (L. Colombera), N.P.Mountney@leeds.ac.uk (N.P. Mountney).

empirical equations (Beard and Weyl, 1973; Hartkamp et al., 1993; McKinley et al., 2011), and this is potentially a cause for significant error. In addition, application of this method requires removing the effects of diagenesis (cements and secondary pores) on porosity (McBride, 1988).

In consideration of these shortcomings, the development of a new method for assessment of compaction is needed. In outcropping fluvial successions, the compacted geometry of channel sandbody margins cut into non-cohesive deposits can be measured, whereas the original (decompact) geometry of these margins can be reconstructed assuming that they approximated the angle of repose of the material they are made of, which can itself be assessed experimentally. Hence, a method is proposed whereby compaction is estimated on the basis of inferred changes in cut-bank geometry resulting from compaction. The aim of this study is to demonstrate a new method based on this principle for the calculation of the compaction in fluvial successions. Specific objectives of this research are as follows: (i) presentation of the theory that underpins the methods; (ii) illustration of how the method is used in practice through its application to a number of fluvial successions; and (iii) comparison and validation of the method against estimations of compactional porosity loss based on thin-section data. The importance of the method for geological research is then discussed.

2. Theory

2.1. Shape of channel banks and their submerged angles of repose

The angle portrayed by erosional channel margins (Φ in Fig. 1a) is related to the submerged angle of repose of the sediments hosting these cut banks (e.g., Glover and Florey, 1951; Ikeda and Izumi, 1991). The relationship between the geometry of channel margins and the related angle of repose of channel-bank sediment needs to be considered with respect to the shape of the channel, to the state of its bed (erosional

or depositional), and to the presence of secondary fluid circulation therein.

For banks composed of uniform, non-cohesive sediments, Glover and Florey (1951) proposed that the ideal cross section of a channel can be expressed as follows:

$$y = h \cos\left(\frac{x}{h} \tan\Phi\right) \quad (1)$$

where h is the maximum bankfull depth (water depth at the thalweg) (Fig. 1a), and Φ is the angle portrayed by the channel margin near the channel top, considered equivalent to the submerged angle of repose of the sediments forming the channel margin (bank). In this equation, the water-flow direction is assumed parallel to the channel path, ignoring the effects of secondary flow. For a section through a stable channel (i.e., undergoing bypass), sediments on the stream bed should be at conditions of critical incipient motion (Glover and Florey, 1951; Ikeda and Izumi, 1991), and so we can consider the equation:

$$F = \tau_c \quad (2)$$

where F is the resultant force, and τ_c is the critical drag force of the channel bed. The resultant force acting upon sediments on the channel bank can be expressed by the following equation (Fig. 1a):

$$F = \sqrt{(G' \sin\theta)^2 + (F_D)^2} \quad (3)$$

where G' is the submerged gravity of the sediments, F_D is the drag force acting on the sediments associated with downstream water flow, and θ is the dip angle of the channel banks. The critical drag force of sediment forming the channel bank is expressed by the following equation:

$$\tau_c = \tan\Phi(G' \cos\theta) \quad (4)$$

where Φ is the submerged angle of repose of the channel-margin sediments. Based on Eqs. (2)–(4) and Fig. 1a, Eq. (1) can be derived (see details in Glover and Florey, 1951). In the Eq. (4), the dip angle of the ideal channel bank at the water surface is equal to the submerged angle of repose of the sediments (Φ) forming the channel margin.

On this basis, we further discuss the channels undergoing erosion or deposition. For channels undergoing erosion, and assuming ideal downstream flow (ignoring the effects of secondary flow), the channel bed will incise while keeping the ideal channel shape (Fig. 1b), minimizing wetted perimeter, bankfull width and cross-sectional area, and maximizing hydraulic efficiency and water depth (Glover and Florey, 1951; Griffiths, 1981; Ikeda and Izumi, 1991). For channels undergoing deposition, the channel bed aggrades, but surfaces of former erosion at channel banks can be preserved in some cases (Nichols and Fisher, 2007; Fielding et al., 2018). Hence, the preserved channel banks are expected to approximate the angle of repose for these situations.

In sandy channel belts, barforms and channel fills characterized by fining-upward grain size trends, even in fully non-cohesive sediments, are common, and these deposits can form the banks of channels eroding into them; this situation is now discussed (Fig. 1c). Near the water surface (i.e., towards the top of the channel) at the bank, the pressure produced by the water column is negligible for the ideal downstream flow (ignoring secondary flow and water diffusion), and so the drag force produced by downstream flow can be ignored (Glover and Florey, 1951; Ikeda and Izumi, 1991); this assumption is in accord with observations based on modern rivers for which the stream-bed shear stress near the water surface in straight reaches of a river is usually negligible (Dietrich and Whiting, 1989; Frothingham and Rhoads, 2003). Hence, Eqs. (3) and (4) can be rewritten as (Glover and Florey, 1951; Ikeda and Izumi, 1991):

$$F = \sqrt{(G' \sin\theta)^2} = \tan\Phi(G' \cos\theta) \quad (5)$$

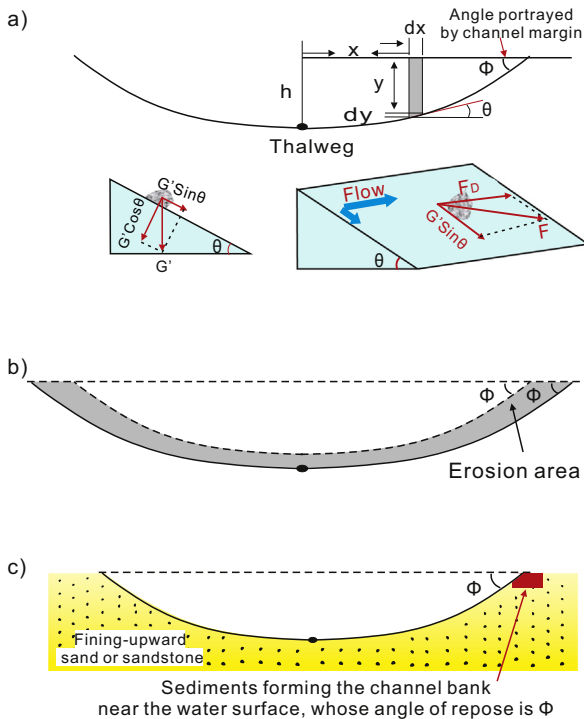


Fig. 1. Channel cross section associated with idealized downstream flow, i.e., without secondary flow. All the three theoretical channel sections form in non-cohesive (sandy) sediments. (a) Ideal channel section with uniform, non-cohesive banks, and its force analysis (modified after Glover and Florey, 1951). (b) Ideal section of a channel undergoing erosion. (c) Section of a channel hosted in fining-upward, non-cohesive sediments.

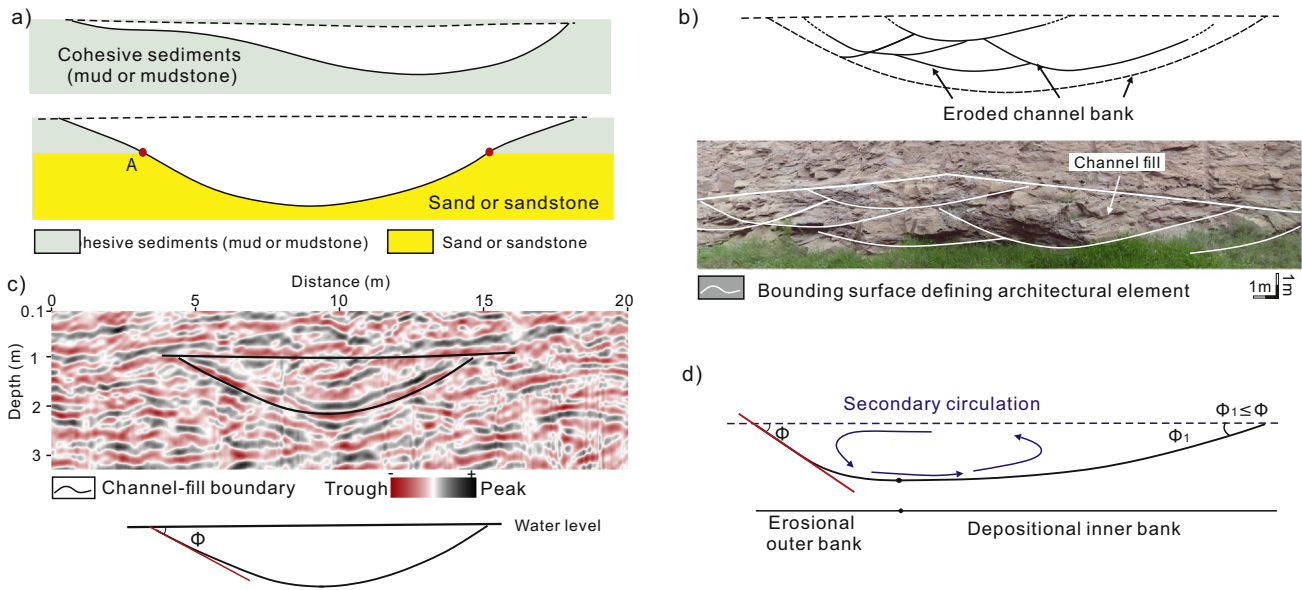


Fig. 2. Four types of common channel sections. (a) Channels with cohesive-sediment banks. The upper sections illustrate examples of channel fills encased in muds or mudstones, based on observations by Nichols and Fisher (2007); the lower section shows a channel form that is partly encased in sands or sandstones but with margins pinching out in muds or mudstones. (b) Eroded channel fills and the photomosaic of eroded channel fills (the outcropping channel fills is part of the outcrop J-RB, see below). (c) Fully preserved, approximately symmetrical channel form with non-cohesive banks (based on observations from a chute channel located in a mid-channel bar of the Songhua River, Northern China; coordinate: 45°5'21.78"N, 124°56'34.38"E). (d) Asymmetrical channel form and analysis of forces acting on its outer bank, based on observations by Yue et al. (2019).

where θ is the dip angle of the channel bank at the water surface, Φ is the submerged angle of repose of the channel-bank sediments (red area in Fig. 1c), and θ is equal to Φ (Fig. 1c).

In summary, for channels that are thought to experience ideal downstream flow, i.e., for which secondary circulation is negligible, the angle of the channel bank at (or near) the water surface (Φ in Fig. 1) can be approximated by the submerged angle of repose of the sediments forming the channel margin. The portion of a channel margin of interest to this study is located near the water surface, and is typically characterized by the maximum observed dip angle of the channel bank measured relative to the channel-fill top; this angle tends to be broadly constant over the short length scales being considered (typically a profile with height of 20–30 cm for channel fills with a thickness of 3 m), and by sediments of similar texture along its profile (red area shown in Fig. 1c).

Real-world fluvial channels can take variable shapes in relation for example to complex secondary flow, scour and erosion, and non-uniformity of bank sediments (Frothingham and Rhoads, 2003; Bertoldi and Tubino, 2005). Considering the nature of the sediments forming the channel bank and the channel cross-sectional shape, four types of channel forms are common, as presented in Table 1 and Fig. 2. Channel banks hosted in fine-grained sediments (clay to medium silt) are not expected to approximate the submerged angle of repose

because of the effects of cohesive forces (see type 1 in Table 1, and Fig. 2a). The angle portrayed by the margins of channel fills incorporated in a fluvial succession whose pinch-outs (i.e., margins at the channel-fill top) are not preserved because of erosion is usually less than the related angle of repose (see type 2 in Table 1, and Fig. 2b). For approximately symmetrical channel forms, a force analysis of the channel banks similar to that presented above for ideal channels can be considered, according to which the angle of the channel (or channel-fill) margin near the water surface (or channel-fill top) approximates the submerged angle of repose (see type 3 in Table 1, and Fig. 2c)

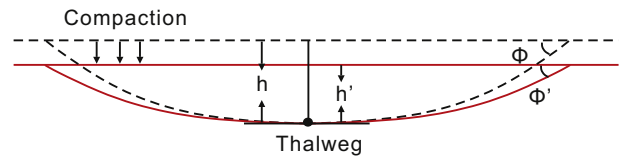


Fig. 3. Schematic diagram showing changes in the angle of repose and thickness arising from compaction. h is the original channel depth, h' is the channel-fill thickness after compaction, Φ is the angle of repose, and Φ' is the angle of the channel-fill margin near its top, which approximates the compacted submerged angle of repose.

Table 1

Classification of channel forms and channel fills based on expected relationships between the angle of their margins and the angle of repose of channel-margin sediments.

Types of channels and channel fills	Sediments of channel margin	Fully preserved or top-truncated	Shape of channel section	Angle of channel margin of outer bank
Type 1 Channel fill with cohesive banks	Cohesive	^a	/	Not related to Φ^b
Type 2 Eroded channel fills	Non-cohesive	Top-truncated	/	Less than Φ
Type 3 Fully-preserved, symmetrical channel fill	Non-cohesive	Fully preserved margin	Approximately symmetrical	Equal to Φ
Type 4 Fully-preserved, asymmetrical channel fill	Non-cohesive	Fully preserved margin	Asymmetrical	Approximately Equal to Φ

Note: Types 3 and 4 are suitable for application of the proposed method because the angle of inclination of their channel margin is expected to approximate the submerged angle of repose.

^a No need to limit this condition.

^b submerged angle of repose of the sediments forming the channel margin.

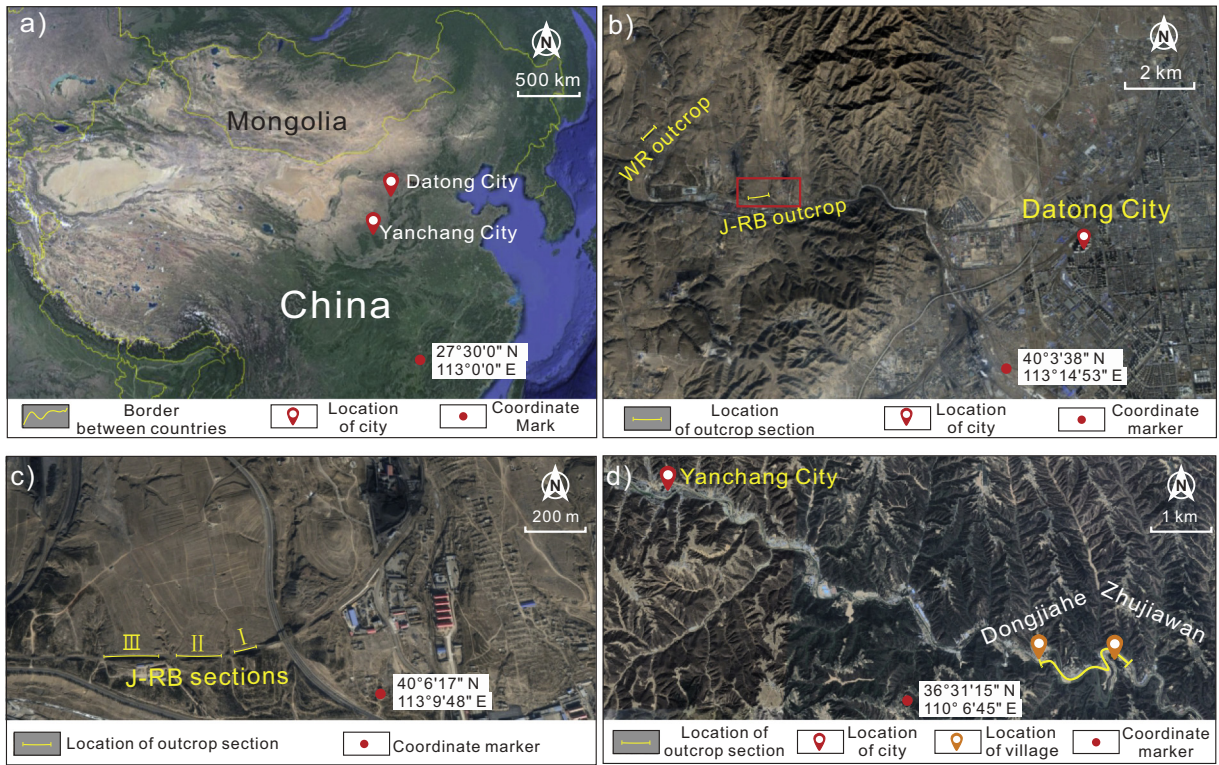


Fig. 4. Satellite images from Google Maps showing the locations of the study outcrops. (a) Locations of Datong City and Yancheng City. (b) Locations of WR outcrop and J-RB outcrop. (c) Position of the three outcropping sections of J-RB outcrop, corresponding to the area in the red frame in panel b. (d) Locations of Yancheng outcrop.

(Glover and Florey, 1951; Ikeda and Izumi, 1991; El Kadi Abderrezak et al., 2016). For asymmetrical channel forms with non-cohesive banks (see type 4 in Table 1), the angle of the channel margin along its outer bank can also be approximated by the submerged angle of repose. In this type of channel, complicated secondary circulation is

common, typically in the form of helical flow (Gessner, 1973; Frothingham and Rhoads, 2003). Commonly, the cross-stream component of secondary circulation is directed upwards along the inner bank, and downwards along the outer bank (van de Lageweg et al., 2014; Baar et al., 2018) (Fig. 2d). Consequently, the secondary flow

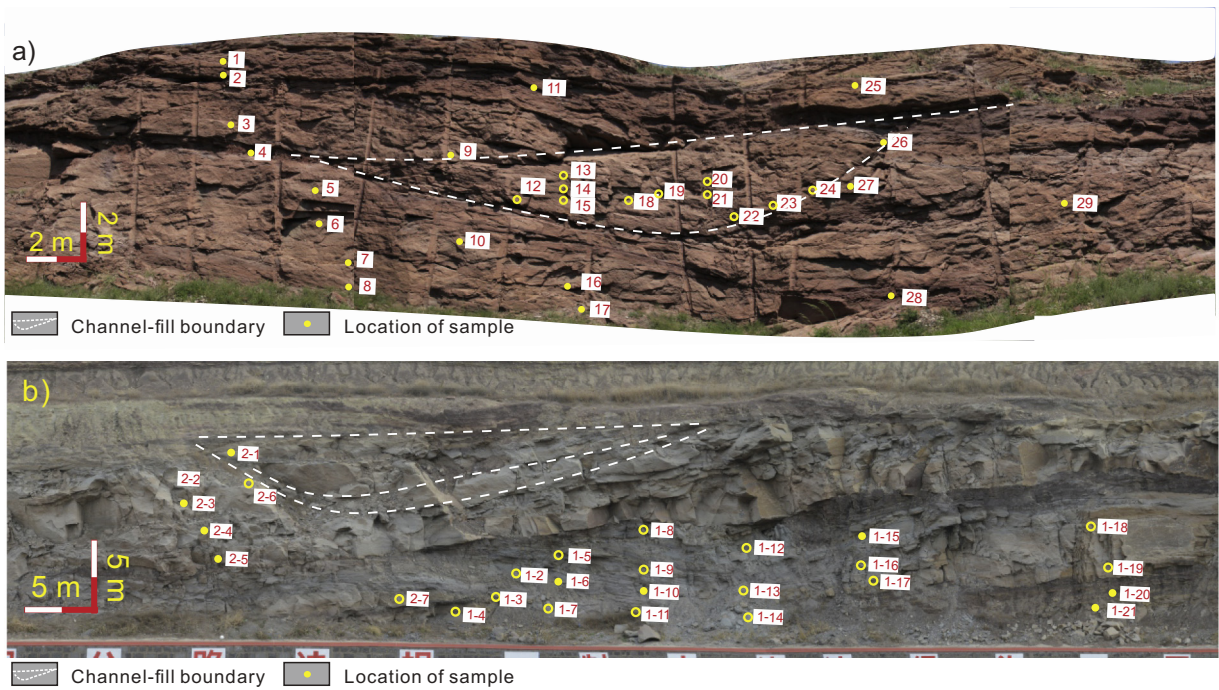


Fig. 5. Locations of some samples to illustrate the sampling procedure. All the samples were employed for grain size analyses; the empty circles show the samples with porosity analyses, conducted using a helium porosimeter. (a) Locations of samples in section II of outcrop J-RB. Submerged angles of repose were measured for samples numbered 26, 27 and 29. (b) Locations of some samples in outcrop WR. Submerged angles of repose were measured for samples numbered 2-1, 2-6 and 1-18.

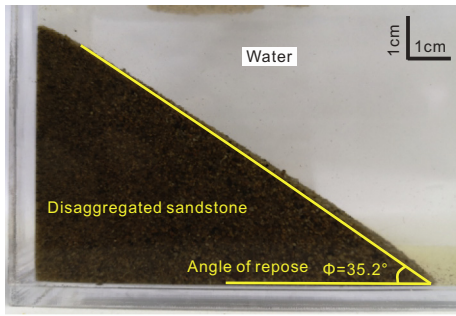


Fig. 6. Photo showing the submerged angle of repose of disaggregated sand grains derived from an original sandstone sample. In this sample the measured angle of repose is 35.2°.

enhances the resultant force acting on the outer bank (Frothingham and Rhoads, 2003; van de Lageweg et al., 2014), which promotes erosion of the outer bank and causes an increase in the steepness of the margin. Hence, the angle of the outer bank is expected to be larger than or equal to the corresponding angle for the idealized channel bank, and to reach its maximum (i.e., the angle of repose) near the water level (Fig. 2d). Nonetheless, the nature of secondary flow in river channels is complex, and in some cases even circulation cells with a downward-directed flow component can develop along the outer banks (Frothingham and Rhoads, 2003). For sake of simplicity, in this work, we ignore the potential effects of secondary flow on channel-bank geometry.

2.2. Estimation of compaction based on changes of submerged angle of repose

For fully preserved channel fills with non-cohesive sediment banks, the angle of the outer-bank margin in proximity of the channel-fill top is

taken as approximately equal to the submerged angle of repose of the channel-margin sediments. The angle exhibited by the present-day channel-fill margin is lower than the angle of the original bank of the formative channel because of compaction (Fig. 3). The original (decompacted) angle is assumed to have been equal to the submerged angle of repose of the non-cohesive bank material. Accordingly, the compaction ratio of the outcropping successions can be calculated using the following equation:

$$C = \frac{h}{h'} = \frac{\tan\Phi}{\tan\Phi'} \tag{6}$$

where *C* is the compaction ratio, *h* is the original channel depth, and *h'* is the compacted channel-fill thickness. Φ is the submerged angle of repose, which can be obtained experimentally. Φ' is the compacted Φ , which can be measured directly from the margins of channel fills observed in outcrop.

3. Geological setting of studied successions

To illustrate and test the above method, this work utilizes three outcropping successions from different geographic regions and different stratigraphic intervals; all three successions are interpreted to be fluvial in origin, though their formative rivers are inferred to have been of different planform types, representative of braided, mixed braided-meandering, and meandering systems.

3.1. Outcrop 1

This outcropping fluvial succession is located to the northwest of Datong City, northern China (Fig. 4a,b), at 40° 6' 19.12" N, 113° 9' 11.57" E. The outcrop is along a railway cutting of the Jinhuaogong colliery, next to a bridge; it is named as Railway & Bridge outcrop (J-RB outcrop). This outcrop consists of 3 sections, with an average height of 8 m, and a total lateral extent of 300 m (Fig. 4c). The outcrops of this succession

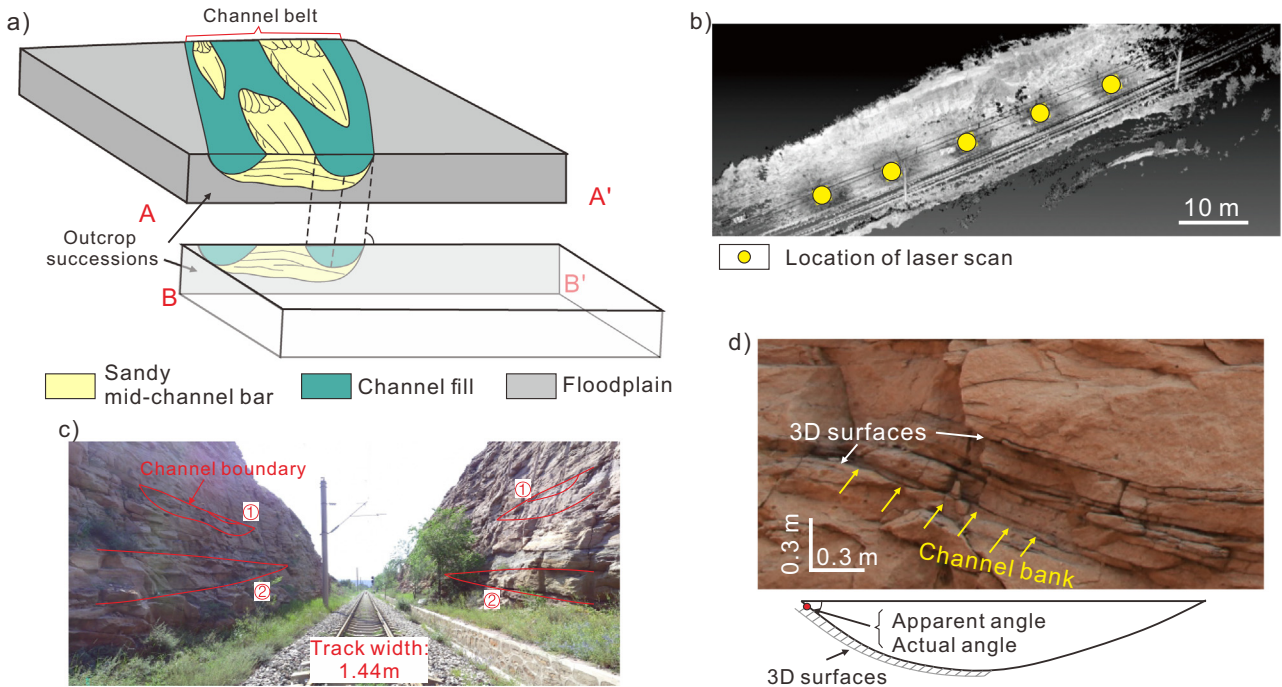


Fig. 7. (a) Map showing the relation between the orientation of some outcropping successions and channel-fill geometry along depositional strike. (b) 3D laser-scan point-cloud data of section II of outcrop J-WR in “bird’s eye” view. Spatial coordinates of measured points are obtained at mm-scale resolution. (c) 3D laser-scan acquisition of the outcrop in part (b), showing two example channel fills recognizable on both sides of the railway cutting (labelled as ‘1’ and ‘2’). (d) Outcrop photo of a channel-bank surface whose small-scale geometry is exposed in 3D from which a true dip angle can be determined.

expose parts of the Jurassic Yungang Formation, which has been interpreted as representative of a sandy braided fluvial system (Li et al., 2015).

3.2. Outcrop 2

This outcropping fluvial succession is located close to the village Wuguantun along the 301 Provincial Road (named as WR outcrop), approximately 5 km to the northwest of the J-RB outcrop, at $40^{\circ} 7' 22.73''$ N, $113^{\circ} 7' 9.81''$ E. This outcrop also exposes parts of the Jurassic Yungang Formation, albeit for a part of the succession that has a different character to that in the J-RB outcrop. The WR outcrop has an average

height of 25 m and a lateral extent of 300 m (Fig. 4b). In this outcrop, a fluvial succession of inferred braided origin is dominant; in the upper part of this succession, an increase in architectural elements interpretable as side-bar deposits represents the possible record of a transition to single-thread planforms (Chen, 2012).

3.3. Outcrop 3

This outcropping fluvial succession is located along the banks of the Yanhe River, approximately 12 km to the southeast of Yanchang City, at approximately $36^{\circ} 32' 2''$ N, $110^{\circ} 7' 50''$ E (Fig. 4d). The outcrop exposes a tight sandstone (whose porosity is lower than 10% and air

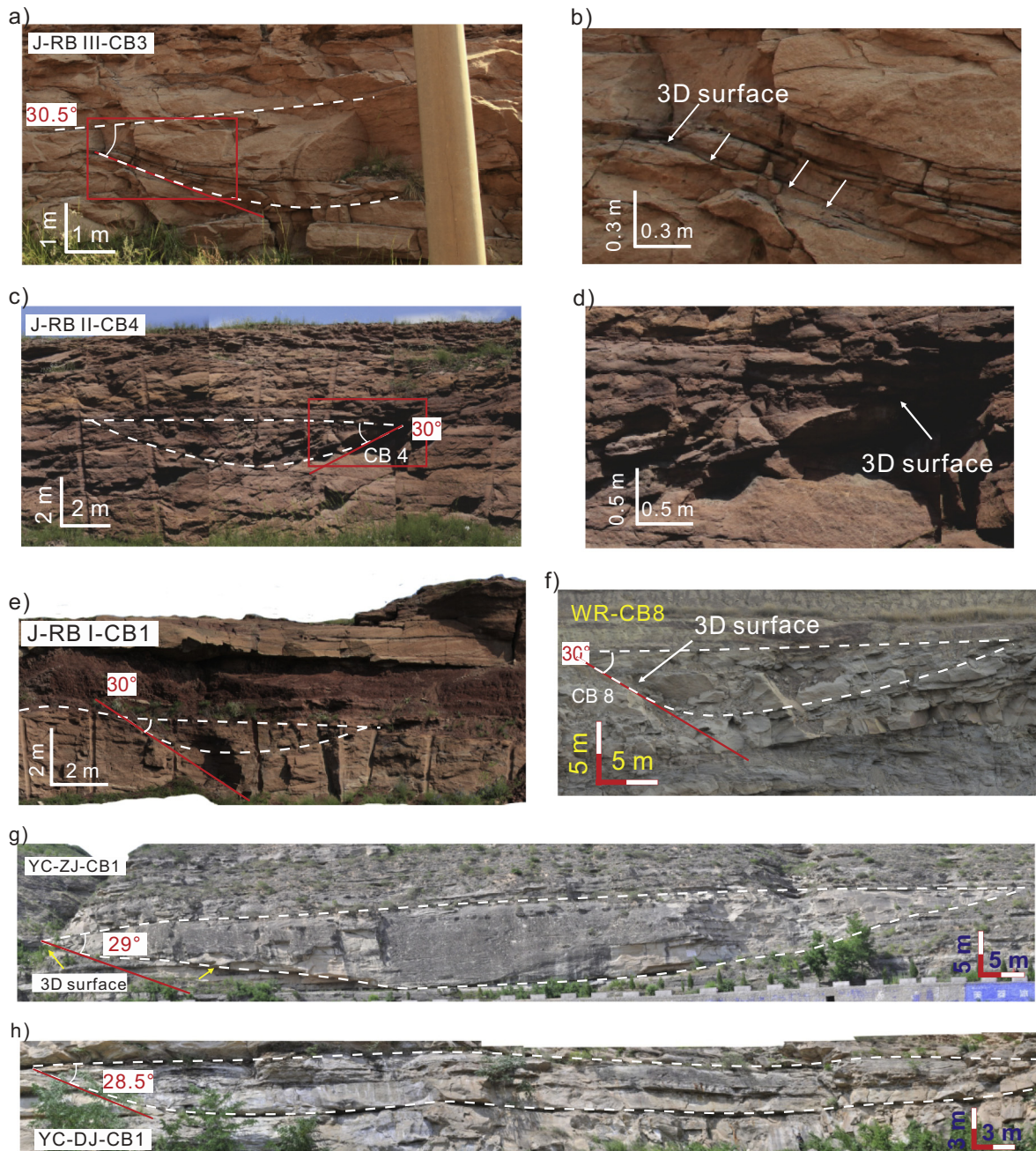


Fig. 8. Photomosaics showing the identified channel fills with non-cohesive banks. (a) An identified channel fill from outcrop J-RB III. (b) Area in the red frame in panel a. (c) An identified channel fill from outcrop J-RB II. (d) Area in the red frame in panel c. (e) An identified channel fill from outcrop J-RB I. (f) An identified channel fill from outcrop WR. (g) An identified channel fill from outcrop YC-ZJ. (h) An identified channel fill from outcrop YC-DJ. The apparent channel-bank angles seen in outcrop have been corrected to obtain true values. The dashed lines represent channel-fill boundaries; tangents to the channel margins of outer banks near the channel-fill tops are shown as red lines. One example from each outcrop section is shown here; outcrop photographs of all the 27 studied examples can be found in the Supplementary material (see Figures DR1–DR5 in the Supplementary material).

permeability is lower than 1 mD) of the Triassic Yanchang Formation (Chang 6 to Chang 8 members; Fu, 2013); this outcrop is therefore named the YC outcrop. Two sections along this outcrop were selected for detailed study. These are near the villages of Dongjiahe (the YCJ-DJ outcrop section) and Zhujiawan (the YC-ZJ outcrop section). These outcropping successions have been interpreted as having been deposited by a meandering river in a delta-plain setting (Fu, 2013; Zhu et al., 2013).

4. Dataset and methods

The dataset used in this research includes (i) outcrop photomosaics, (ii) data obtained from analyses of rock samples, consisting of measurements of grain size, porosity, and bulk and skeletal density, (iii) impregnated thin sections, and (iv) experimental observations on submerged angles of repose. Three-dimensional laser-scan (FARO Focus3D X330) acquisitions of outcrops J-RB and WR were taken in the field. Grain-size analyses were conducted on 114 sandstone samples: 57 samples from the J-RB outcrop, 41 from the WR outcrop, and 16 from the YC outcrop. Analyses of porosity and bulk and skeletal densities were performed on 27 samples from the J-RB outcrop, 25 samples from the WR outcrop, and 16 samples from the YC outcrop. The samples used for porosity measurements for rocks from outcrops of WR and J-RB were also used for preparing impregnated thin sections. Submerged angles of repose were measured for disaggregated sediments relating to 22 rock samples, of which nine, eleven and two samples are from outcrops J-RB, WR and YC, respectively. The rock samples used for measuring the submerged angle of repose were taken from parts of the channel-fill

margins located near the channel-fill tops. Illustrations of the sampling strategy are shown in Fig. 5.

Sediment grain-size distributions were analyzed using a laser particle analyzer, and porosities were measured using a helium porosimeter. Measurements of submerged angles of repose were carried out for volumes of disaggregated sandstone samples (Fig. 6). The sandstones were disaggregated into their constituent grains employing a method used for particle-size analyses of clastic rocks, consisting of (i) the initial subdivision of the samples into centimeter-scale volumes, which are then (ii) subject to chemical removal of organic matter and cements to loosen the grains, (iii) cleansing of the chemical solvent, and (iv) physical disaggregation by means of rubber sticks (see details in Oil and Gas Industry Standards of China, Xu et al., 2009). This method is widely employed in the particle-size analyses of clastic cores by hydrocarbon exploration and production companies, and has the advantage of imparting negligible physical comminution of the constituent grains (Fu, 2013). Additional grain-size and porosity data for rocks from outcrop YC-ZJ were previously published by Zhu et al. (2013).

Twenty-seven channel-bank angles were measured near channel-fill tops in the three outcropping successions. In cases where the channel fill was not oriented along its strike (cross-stream) section (Fig. 7a), the measured apparent angle was corrected to derive the true channel-bank angle. Two methods were used to correct apparent angles measured in outcrop: (i) for outcrops WR and J-RB, which occur along both sides of road and railroad cuttings, the same channel fill can be recognized on both parallel-trending outcrop sections and analysis of the 3D laser-scan data enabled the channel-fill orientations to be determined precisely (Fig. 7b,c); (ii) for several channel fills (14

Table 2

Assessment of compaction of 27 channel fills using the proposed method, consisting of experimental angle of repose, measured channel-bank angle, and compaction ratio as original to compacted channel-fill thickness.

Channel bank ID	Sandstone sample ID	D ₅₀ ^a (mm)	So ^b	Experimental angle of repose (°) (±0.2°)	Angle of repose of similar samples (°)	Measured channel-bank angle (°) (±0.5°)	Ratio of original to compacted thickness	Average ratio for each outcrop
Outcrop J-RB								
J-RB-I-CB1	J-RB-I-5	0.374	1.595	35.5	/ ^c	30	1.24	
J-RB-II-CB1	J-RB-II-26	0.614	1.487	36	/	31	1.21	
J-RB-II-CB2	J-RB-II-29	0.776	1.530	36.2	/	30.5	1.24	
J-RB-II-CB3	J-RB-II-29	0.776	1.530	36.2	/	30.5	1.24	
J-RB-II-CB4	J-RB-II-30	0.724	1.613	No data	36.2	30	1.27	1.24
J-RB-III-CB1	J-RB-III-6	0.635	1.747	36	/	30.5	1.23	
J-RB-III-CB2	J-RB-III-3	0.813	1.454	No data	36.2	30.5	1.24	
J-RB-III-CB3	J-RB-III-2	0.882	1.443	36.2	/	30.5	1.24	
J-RB-III-CB4	J-RB-III-8	0.658	1.639	No data	36	30	1.26	
Outcrop WR								
WR-CB3	WR-6-2	0.388	1.784	35.7	/	30	1.24	
WR-CB4	WR-7-1	0.335	1.404	35.7	/	29.5	1.27	
WR-CB5	WR-7-5	0.334	1.820	No data	35.7	30	1.24	
WR-CB7	WR-2-1	0.395	1.762	35.7	/	29.5	1.27	
WR-CB8	WR-2-6	0.437	1.500	35.8	/	30	1.25	
WR-CB12	WR-7-4	0.319	1.844	No data	35.6	30.3	1.23	
WR-CB13	WR-7-3	0.316	1.907	35.5	/	30.5	1.21	1.23
WR-CB1	WR-3-5	0.196	1.605	35	/	30	1.21	
WR-CB2	WR-3-6	0.235	1.680	35.1	/	30	1.22	
WR-CB9	WR-3-4	0.242	1.472	No data	35	29.5	1.24	
WR-CB10	WR-3-2	0.261	1.469	35.3	/	30	1.23	
WR-CB11	WR-3-3	0.246	1.589	No data	35	29.8	1.22	
WR-CB14	WR-3-1	0.242	1.866	35.2	/	30	1.22	
Outcrop YC								
DJ-CB1	DJ-3	0.28	1.630	35	/	28.5	1.29	
DJ-CB2	DJ-1	0.23	1.545	35	/	28.5	1.29	
DJ-CB3	DJ-2	0.21	1.491	No data	35	29	1.26	
ZJ-CB1	ZJ-1	0.25	No data	No data	35	29	1.26	1.28
ZJ-CB2	ZJ-2	0.26	1.559	No data	35	28.5	1.29	

^a Is the medium grain diameter.

^b Is the Trask sorting coefficient.

^c Data are unnecessary because the related sample already has measured data.

out of 27) the nature of the outcrops allowed the 3D shape of their channel surfaces to be recognized (Fig. 7d), allowing apparent angles to be corrected trigonometrically.

5. Results

5.1. Estimation of sediment compaction based on changes in channel-bank geometry

In the three outcrops, 27 channel fills with fully preserved banks cut into non-cohesive sandy material were identified (Fig. 8, Table 2). The

submerged angles of repose for the grains forming the banks were measured in experiments (Fig. 6). For cases where the mineral composition, rounding, sorting, and grain-size distribution (D50 and So, i.e., median grain size and Trask sorting coefficients) of sandstone samples are similar, angles of repose of their grains should be similar (El Kadi Abderrezzak et al., 2016; Al-Hashemi and Al-Amoudi, 2018). Hence, when the submerged angle of repose of sediments forming a channel bank was not measured experimentally, the angle of repose determined for rocks with a similar grain-size distribution was considered.

Compaction ratios estimated for the studied channel fills using the proposed method are reported in Table 2. Generally, the ratio

Table 3
Validated assessment of compaction of the three outcrop successions, consisting of estimated original porosity, compactional porosity loss, and compaction ratio of original to compacted thickness.

Sandstone sample ID	So ^a	Porosity determined by He porosimetry (%)	Estimated original porosity (%)	Compactional porosity loss (%)	Ratio of original to compacted thickness	Average ratio for each outcrop	
Outcrop J-RB							
J-RB-I-1	1.850	7.7	33.29	20.9	1.26	1.27	
J-RB-I-3	1.669	8.6	34.63	21.6	1.28		
J-RB-I-4	1.680	8.3	34.54	21.7	1.28		
J-RB-II-12	1.751	10.9	33.99	18.6	1.23		
J-RB-II-13	1.443	11.9	36.78	21.1	1.27		
J-RB-II-14	1.747	8.3	34.02	21.2	1.27		
J-RB-II-15	1.945	6.5	32.68	21.3	1.27		
J-RB-II-16	1.747	7.7	34.02	21.7	1.28		
J-RB-II-17	1.922	7.2	32.82	20.5	1.26		
J-RB-II-18	1.639	7.0	34.89	23.3	1.30		
J-RB-II-20	1.832	8.4	33.41	20.3	1.26		
J-RB-II-28	1.715	8.2	34.26	21.5	1.27		
J-RB-II-29	1.792	8.0	33.69	21.1	1.27		
J-RB-II-3	1.837	7.4	33.38	21.3	1.27		
J-RB-III-2	1.443	9.1	36.78	23.7	1.31		
J-RB-III-3	1.454	8.9	36.66	23.7	1.31		
J-RB-III-4	1.691	7.9	34.45	22.1	1.28		
J-RB-III-5	1.708	8.4	34.32	21.4	1.27		
J-RB-III-8	1.639	7.9	34.89	22.5	1.29		
Outcrop WR							
WR-1-5	1.680	9.8	34.54	20.4	1.26		1.26
WR-1-8	1.866	11.2	33.19	17.1	1.21		
WR-1-9	1.469	12.8	36.50	19.8	1.25		
WR-1-10	1.589	11.8	35.32	19.3	1.24		
WR-1-11	1.588	11.8	35.33	19.3	1.24		
WR-1-12	1.690	6.5	34.46	23.3	1.30		
WR-1-13	1.500	9.9	36.18	22.1	1.28		
WR-1-15	1.762	7.4	33.90	21.8	1.28		
WR-1-16	2.233	7.2	31.17	18.5	1.23		
WR-1-17	1.549	7.2	35.70	23.9	1.31		
WR-6-2	1.784	6.0	33.75	23.0	1.30		
WR-7-1	1.844	6.7	33.33	21.8	1.28		
WR-2-6	1.683	8.3	34.51	21.8	1.28		
WR-2-1	1.724	9.2	34.19	20.5	1.26		
WR-7-4	1.907	5.6	32.92	22.4	1.29		
WR-7-3	1.844	8.3	33.33	20.2	1.25		
WR-7-5	1.820	9.2	33.49	19.7	1.24		
WR-3-5	1.605	10.8	35.18	20.2	1.25		
WR-3-6	1.680	11.4	34.54	19.8	1.25		
WR-3-4	1.779	11.8	33.78	17.4	1.21		
WR-3-2	1.469	11.5	36.50	21.1	1.27		
WR-3-3	1.589	10.9	35.32	20.3	1.25		
WR-3-1	1.477	10.5	36.42	22.0	1.28		
Outcrop YC							
C6-1	1.584	5.3	35.37	23.8	1.31	1.30	
C6-2	1.693	6.6	34.43	22.4	1.29		
C6-3	1.593	6.5	35.29	23.1	1.30		
C6-4	1.493	7.5	36.25	23.3	1.30		
C6-5	1.541	6.4	35.77	23.5	1.31		
C6-6	1.604	7.0	35.18	22.7	1.29		
C6-7	1.502	6.0	36.16	24.1	1.32		
C6-8	1.617	6.3	35.08	23.0	1.30		
C6-9	1.756	6.3	33.95	22.1	1.28		
C6-10	1.511	8.2	36.07	22.8	1.29		

^a So is the Trask sorting coefficient.

of compaction estimated for outcrops J-RB and WR is similar, with values ranging between 1.21 and 1.27, and an average value of 1.24. The studied interval of the Chang 6 Member of the Triassic Yanchang Formation (Ordos Basin) returns a higher estimated compaction ratio compared with the J-RB and WR outcrops, with an average value of 1.28 (Table 2).

5.2. Validation of compaction estimates based on changes of porosity

Sandstone compaction for outcrops WR, J-RB and YC can also be estimated according to changes of porosity resulting from compaction (Table 3). Ignoring compaction and tectonic stress effects, porosity

changes are primarily affected by cementation and secondary dissolution.

In this work, the original porosity of the sandstones (i.e., the porosity of corresponding unlithified sands, pre-burial) was estimated using the empirical equation proposed by Beard and Weyl (1973):

$$Po = 20.91\% + \frac{22.90}{So}\% \tag{7}$$

and considering that:

$$So = \sqrt{D_{25}/D_{75}} \tag{8}$$

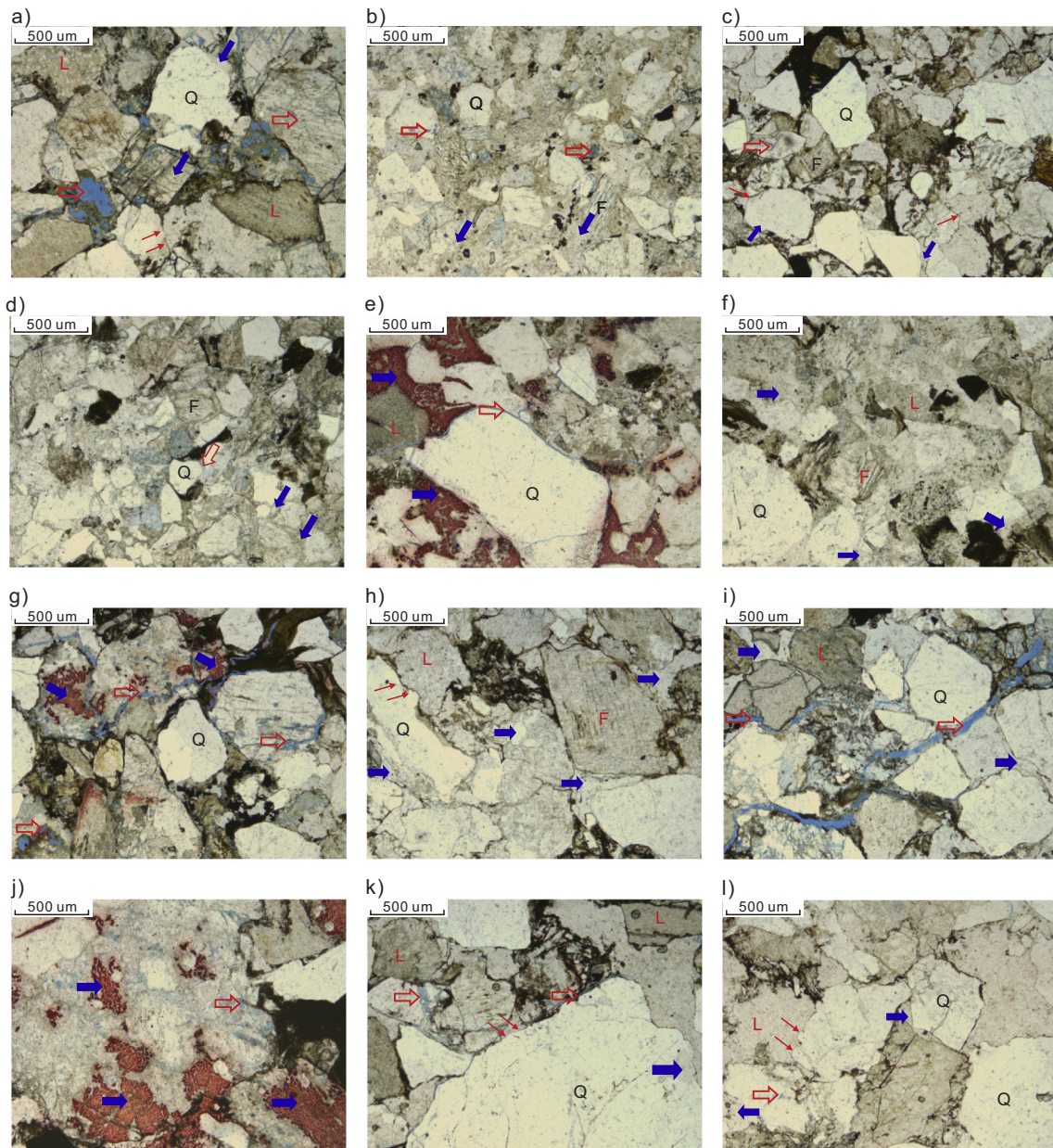


Fig. 9. Thin sections of sandstone samples from the Jurassic Yungang Formation. Samples in parts (a–f) are from outcrop WR. Samples in parts (g–l) are from outcrop J-RB. Components are labelled as follows: Q = quartz; F = feldspar; L = rock fragment. The blue arrows show examples of cements, the red empty arrows illustrate examples of dissolved pores and fractures, and the thin red arrows indicate concave-convex grain contacts. These thin sections indicate that the succession experienced relatively strong cementation (pervasive in example in part d) and compaction (as evidenced by concave-convex grain contacts). Most early dissolution pores were also filled by cement.

where P_0 is the original porosity, S_0 is the Trask sorting coefficient, and D_{25} and D_{75} are the 25th and 75th percentiles of the grain size distribution expressed in millimeters. The overall porosity loss is usually estimated as follows (Ehrenberg, 1989, 1995):

$$\Delta P = P_0 - P_r \quad (9)$$

and considering that:

$$P_r = \frac{IGV(1-P_0)}{1-IGV} \quad (10)$$

$$IGV = P + (\Delta P_2 - \Delta P_3) \quad (11)$$

where ΔP is the compactional porosity loss, P_0 is the original porosity, IGV is the present intergranular volume (as determined in thin sections), P_r is the relative IGV to the original (decompacted) volume, P is the present porosity (as determined as He porosity), ΔP_2 is porosity loss due to cementation, and ΔP_3 porosity gain due to dissolution (mainly intragranular dissolution pores). In these equations, the solid volume is assumed constant.

For outcrops WR and J-RB, thin sections indicate that the majority of the intergranular volume is filled with cement (Fig. 9). Since most secondary pores are also infilled by cements, overall estimations are made for the proportion of features related to cementation and dissolution in the 47 thin sections (Fig. 10a), whose mean value is 7.9% (relative to thin-section area), approximately equal to 6% of the original volume (Eq. (10)). For the tight sandstone of outcrop YC, thin sections with which to estimate the proportion of porosity change resulting from compaction and diagenetic processes were not available, but existing studies on the reservoir quality of tight sandstone in the Yanchang Formation in the Ordos Basin (Fu, 2013; Zhu et al., 2013; Zhang et al., 2014; Li, 2018; Wang et al., 2019) indicate that the compactional porosity loss typically accounts for 75% (median value; range 19–96%; mean 74%) of the overall porosity loss (Fig. 10b). Using this median value, we calculated the compactional porosity loss and the ratio of original to compacted thickness (Table 3).

6. Discussion

6.1. Validation of the method against results of a conventional approach

Estimations of compaction based on the proposed method were compared with results of the method based on compactional porosity loss. The average ratios of original to compacted thickness of the three outcrop successions are 1.24, 1.23 and 1.28 (Table 2), respectively, as based on the proposed method, compared to average ratios equal to 1.27, 1.26 and 1.30 (Table 3), respectively, as derived using the conventional method. Thus, the two approaches return similar compaction estimates, with discrepancy in mean values generally below 0.03.

In most cases, for each sandstone sample, more than a single porosity analysis was performed, so a range of values of the ratio of original to compacted thickness was derived based on porosity change for these channel fills. A comparison between the results of the two methods indicates that compaction estimations are broadly similar (Fig. 11). Compaction estimations for strata of the J-RB outcrop (orange dots in Fig. 11a) show slightly larger discrepancies between the two methods than the other two outcrop datasets (WR and YC outcrops; black and blue dots, respectively, in Fig. 11a), but still with discrepancies mainly below 0.03. For each channel fill, ratios of original to compacted thickness derived using the proposed method and corresponding average values of these ratios based on compactional porosity loss demonstrate a positive correlation, with a Pearson's correlation coefficient of 0.91 (P -value < 0.001; Fig. 11b). The discrepancies between the values yielded by the two methods are <0.03 for 26 of the 27 channel fills (Fig. 11b).

The proposed method tends to return estimated compaction ratios that are slightly smaller than those obtained using the conventional method, but it is difficult to determine which method is more prone to error. The methods based on compactional porosity loss is potentially subject to errors relating to estimation of original porosity, and the ways in which cements and secondary pores are accounted for. Likewise, errors in the estimation of compaction from inferred changes in channel-fill geometry might potentially arise from the theoretical simplifications made above and limitations in the outcrop datasets to which the method is applied. Yet, a significant advantage of the proposed method is that all the parameters that are necessary for its application can be measured in outcrop, with the conditions that the true orientation of channel fills can be directly determined or inferred, and

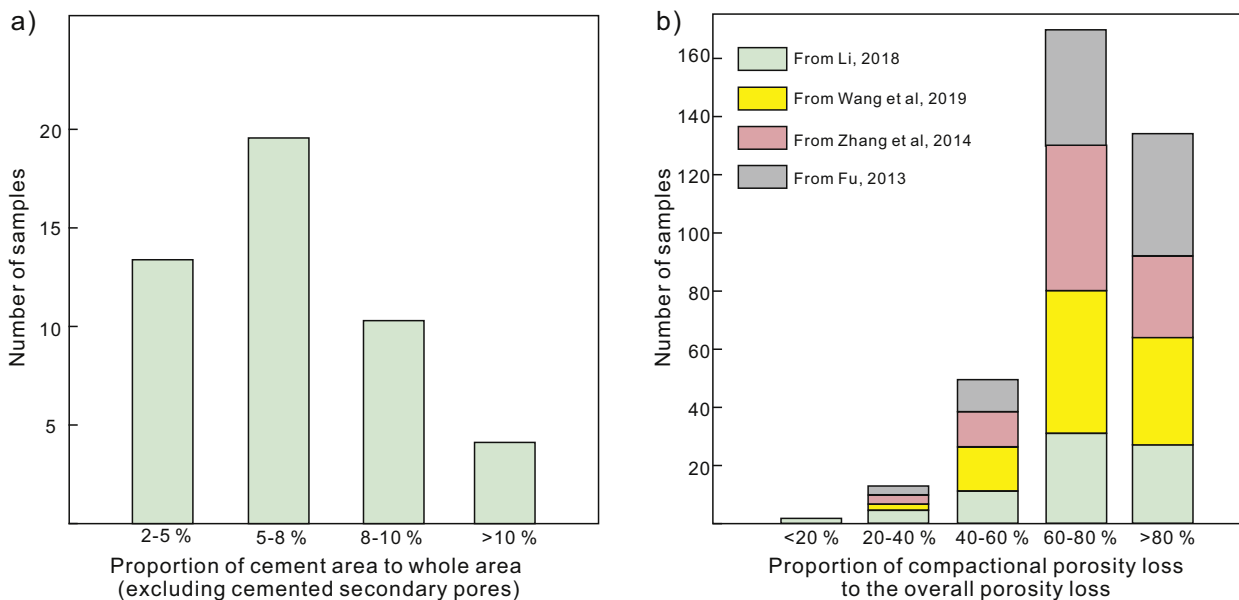


Fig. 10. (a) Bar chart of areal proportions of cemented pores for 47 sandstone thin sections. These statistics do not include cement-filled secondary-pore volume, because this volume does not affect the original solid volume. (b) Bar chart of compactional porosity loss relative to the overall porosity loss. The bars are color-coded by primary data sources, as in legend.

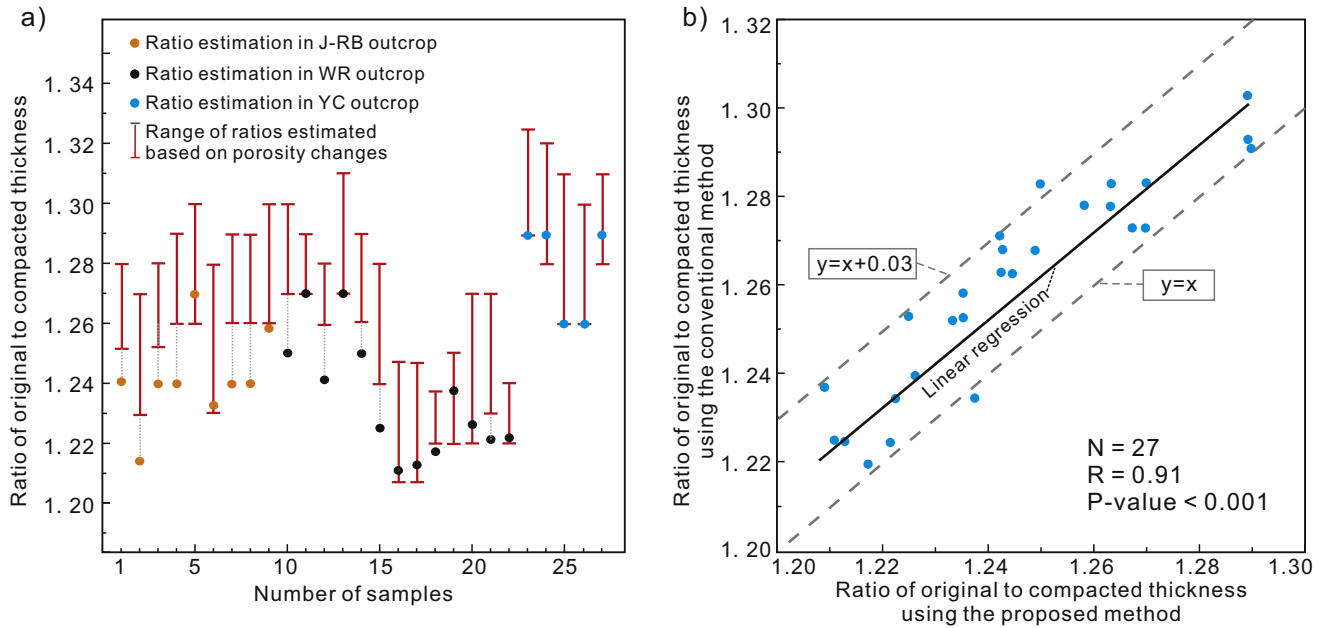


Fig. 11. Comparison between estimations of compaction using the proposed method and estimations made with a conventional method based on thin-section observations of porosity change. (a) Plot of original to compacted thickness ratios for each channel fill; the spots, color-coded by outcrop, report values calculated according to the proposed method, i.e., based on the inferred change of channel-margin geometry, whereas the red bars present ranges based on the compactional porosity loss. The discrepancies between results of the two methods are below 0.03. (b) Cross-plot between the thickness ratio estimated for each channel fill using the proposed method (x axis) and the corresponding average ratio derived using the conventional method (y axis). N is the number of samples; R is the Pearson's correlation coefficient; the P-value, being < 0.01 (2-tailed), indicates statistical significance of the correlation. (For interpretation of the references to color in this figure, the reader is referred to the web version of this article.)

that suitable experimental data on submerged angles of repose of analog sediments exist. The broad convergence in estimation results obtained with the two methods (Fig. 11) suggests that the proposed method can be readily applied to the estimation of compaction for outcropping fluvial successions.

6.2. Applications of the method

The proposed method relies on observation of the true dip angle of a preserved channel bank near the channel-fill top and pinch-out position. The method can be of use in application to integrated subsurface datasets. For example, channel fills are imaged in ground-penetrating radar (GPR) datasets of sand-prone shallow successions (e.g., Lunt et al., 2004), and some 3D seismic datasets exist of sand-rich channel belts, especially for the shallow subsurface (e.g., Zhuo et al., 2015; Durkin et al., 2017); the method can be applied to depth-converted geophysical data. More importantly, however, the method is readily applicable in outcrop studies. Decompaction of sandbodies, as allowed by this approach, is useful to a range of geological disciplines.

The method can benefit studies that rely on the characterization of the geometry of fluvial architectural elements, such as paleohydrological investigations attempting inference of changes in river hydrology and associated paleoclimatic conditions based on estimations of channel hydraulic geometry derived from channel-fill architectures (e.g., estimation of maximum bankfull depth from channel-fill thickness or mean depth from dune-scale cross-set thickness; cf. Mohrig et al., 2000; Leclair and Bridge, 2001; Colombera et al., 2017). This is particularly important for comparisons between successions that have undergone variable degree of compaction, especially if compared with modern rivers (e.g., Ielpi et al., 2017; Ganti et al., 2019): corrections operated according to the suggested method should permit more accurate and meaningful comparisons between depositional systems. Furthermore, quantification of the degree of compaction of sandbodies can be used to attempt restoration of the original

decompact thickness of entire stratigraphic intervals of fluvial successions, based on knowledge of their sandstone-to-mudstone ratios (Perrier and Jacques, 1974). In turn, these estimations should facilitate and improve comparisons between different successions, if these need to be evaluated with respect to their original aggradation rates (e.g., Colombera et al., 2015; Schwartz et al., 2017). For purposes of basin analysis, improved estimations of the original thickness of clastic strata can be employed to refine estimations of rates of tectonic subsidence in sedimentary basins.

6.3. Limitations of the method

A primary limitation of the method is that the original bank geometry may be modified by tectonic shearing. In such a scenario, which may not be readily diagnosed, this method is not applicable.

Furthermore, application of the method requires channel fills (see Table 1) whose full channel forms are preserved, and for which the true angles of channel banks can be measured or calculated from apparent angles (see details in Section 4). However, reconstruction of channel-fill orientation is often challenging in outcrop studies and full channel-form preservation may be rare in amalgamated sand-prone successions.

More fundamentally, however, channel banks may develop that do not approximate – in their upper part – the angle of repose of the sediment in which they are carved, in some cases because of the effects of complex secondary flow (Frothingham and Rhoads, 2003), and this is likely to be a source of error. Although it is not possible for us to quantify this error, the effect of secondary circulation should be negligible for symmetrical and approximately symmetrical channel fills. For this reason, it is preferable to sample symmetrical or approximately symmetrical channel fills, which may represent the infill of relatively low-sinuosity channels, chute channels, or riffle zones of meandering channels. Moreover, the uppermost parts of banks can be subject to deformation arising from liquefaction

(especially for fine-sediment banks) (Wotherspoon et al., 2012) or may be contained in capillary zones.

7. Conclusions

- 1) A new method for estimating the sediment compaction of sand bodies in fluvial successions is proposed. The compacted geometry of channel margins cutting into non-cohesive deposits can be measured in outcropping fluvial successions, whereas the decompact angle of repose of the sediment forming these margins can be estimated experimentally. Assuming the upper part of the channel bank to have formed at its angle of repose, sediment compaction can be calculated on the basis of the compacted channel-bank angle and the corresponding angle of repose.
- 2) The proposed method is applied to three outcropping successions from different geographic regions and different stratigraphic intervals. Compaction estimates of the three successions are also made using a conventional method for determining compactional porosity loss based on thin-section observations and helium-porosity readings. The estimates of compaction obtained with the two methods are similar, indicating that the proposed method is suitable for the assessment of compaction in outcropping fluvial successions.
- 3) Compared to other established methods, all the parameters that are necessary for applying the proposed method can be obtained through outcrop studies, or through other forms of investigation suitable for elucidating the architecture and lithology of fluvial channel fills and their banks (e.g., integrated core and GRP or shallow-seismic datasets). Nonetheless, some error is likely to be introduced by the theoretical simplification of considering channel banks as having developed at the angle of repose, and there exist practical limitations to the applicability of the proposed method, chiefly the need for observations on fully preserved, tectonically undeformed channel fills cutting into non-cohesive deposits, forming banks whose geometry can be seen or inferred.

Acknowledgments

This study was financially supported by the National Natural Science Foundation Project of China (No. 41872107), Cooperation Project of the PetroChina Corporation (ZLZX2020-02-02-02) and National Major Science and Technology Project of China (No. 2017ZX05009001-002). WL was financially supported by China Scholarship Council. LC and NPM thank the sponsors and partners of FRG-ERG for financial support: AkerBP, Areva (now Orano), BHPBilliton, Cairn India (Vedanta), ConocoPhillips, Chevron, Equinor, Murphy Oil, Nexen-CNOOC, Occidental, Petrotechnical Data Systems, Saudi Aramco, Shell, Tullow Oil, Woodside and YPF. We also thank Jasper Knight (Editor in Chief) and an anonymous reviewer for their valuable comments, which helped us improve our manuscript.

Appendix A. Supplementary data

Supplementary data to this article can be found online at <https://doi.org/10.1016/j.sedgeo.2020.105675>.

References

- Al-Hashemi, H.M.B., Al-Amoudi, O.S.B., 2018. A review on the angle of repose of granular materials. *Powder Technol.* 330, 397–417.
- Athy, L.F., 1930. Density, porosity, and compaction of sedimentary rocks. *J. Vacat. Mark.* 3, 234–244.
- Baar, A.W., de Smit, J., Uijtewaal, W.S.J., Kleinans, M.G., 2018. Sediment transport of fine sand to fine gravel on transverse bed slopes in rotating annular flume experiments. *Water Resour. Res.* 54, 19–45.
- Beard, D.C., Weyl, K.P., 1973. Influence of mineralogy and texture on porosity and permeability of diatomites. *Am. Assoc. Pet. Geol. Bull.* 57, 349–369.
- Bertoldi, W., Tubino, M., 2005. Bed and bank evolution of bifurcating channels. *Water Resour. Res.* 41, 1–12.
- Bridge, J.S., Lunt, I.A., 2006. Depositional models of braided rivers. In: Smith, G.H.S., Best, J.L., Bristow, C.S., Petts, G.E., Jarvis, I. (Eds.), *Braided Rivers*. Blackwell, Oxford, pp. 11–50.
- Chen, Y., 2012. Architecture Characterize for Sandy Braided River Reservoir. [Ph.D. thesis]. China University of Petroleum, Beijing.
- Colombera, L., Mountney, N.P., McCaffrey, W.D., 2015. A meta-study of relationships between fluvial channel-body stacking pattern and aggradation rate: Implications for sequence stratigraphy. *Geology* 43, 283–286.
- Colombera, L., Arévalo, O.J., Mountney, N.P., 2017. Fluvial-system response to climate change: the Paleocene-Eocene Tremp Group, Pyrenees. Spain. *Glob. Planet. Change* 157, 1–17.
- Dietrich, W.E., Whiting, P., 1989. Boundary shear stress and sediment transport in river meanders of sand and gravel. In: Ikeda, S., Parker, G. (Eds.), *Meandering Rivers*. American Geophysical Union, Florida, pp. 1–50.
- Durkin, P.R., Boyd, R.L., Hubbard, S.M., Shultz, A.W., Blum, M.D., 2017. Three-dimensional reconstruction of meander-belt evolution, Cretaceous McMurray Formation, Alberta Foreland Basin. Canada. *J. Sediment. Res.* 87, 1075–1099.
- Ehrenberg, S.N., 1989. Assessing the relative importance of compaction processes and cementation to reduction of porosity in sandstones: discussion; compaction and porosity evolution of Pliocene sandstones, Ventura basin, California: discussion. *Am. Assoc. Pet. Geol. Bull.* 73, 1274–1276.
- Ehrenberg, S.N., 1995. Measuring sandstone compaction from modal analyses of thin sections: how to do it and what the results mean. *J. Sediment. Res.* A65, 369–379.
- El Kadi Abderrezzak, K., Die Moran, A., Tassi, P., Ata, R., Hervouet, J.-M., 2016. Modelling river bank erosion using a 2D depth-averaged numerical model of flow and non-cohesive, non-uniform sediment transport. *Adv. Water Resour.* 93, 75–88.
- Fielding, C.R., Alexander, J., Allen, J.P., 2018. The role of discharge variability in the formation and preservation of alluvial sediment bodies. *Sediment. Geol.* 365, 1–20.
- Frothingham, K.M., Rhoads, B.L., 2003. Three-dimensional flow structure and channel change in an asymmetrical compound meander loop, Embarras River, Illinois. *Earth Surf. Process. Landforms* 28, 625–644.
- Fu, J., 2013. Research on Reservoir Architecture and Quality Difference of Shallow-water Delta: A case of the Yanchang Formation in Ordos Basin. [Ph.D. thesis]. China University of Petroleum, Beijing.
- Ganti, V., Whittaker, A.C., Lamb, M.P., Fischer, W.W., 2019. Low-gradient, single-threaded rivers prior to greening of the continents. *Proc. Natl. Acad. Sci. U. S. A.* 116, 11652–11657.
- Gessner, F.B., 1973. The origin of secondary flow in turbulent flow along a corner. *J. Fluid Mech.* 58, 1–25.
- Glover, R.E., Florey, Q.L., 1951. Stable Channel Profiles. U.S. Bureau of Reclamation, Hydraulic Laboratory Report No. Hyd-325.
- Griffiths, G.A., 1981. Stable-channel design in gravel-bed rivers. *J. Hydrol.* 52, 291–305.
- Hartkamp, C.A., Arribas, J., Tortosa, A., 1993. Grain size, composition, porosity and permeability contrasts within cross-bedded sandstones in Tertiary fluvial deposits, central Spain. *Sedimentology* 40, 787–799.
- Ielpi, A., Rainbird, R.H., Ventra, D., Ghinassi, M., 2017. Morphometric convergence between Proterozoic and post-vegetation rivers. *Nat. Commun.* 8, 1–8. <https://doi.org/10.1038/ncomms15250>.
- Ikeda, S., Izumi, N., 1991. Stable channel cross sections of straight sand rivers. *Water Resour. Res.* 27, 2429–2438.
- van de Lageweg, W.I., van Dijk, W.M., Baar, A.W., Rutten, J., Kleinans, M.G., 2014. Bank pull or bar push: what drives scroll-bar formation in meandering rivers? *Geology* 42, 319–322.
- Leclair, S.F., Bridge, J.S., 2001. Quantitative interpretation of sedimentary structures formed by River Dunes. *J. Sediment. Res.* 71, 713–716.
- Li, Z., 2018. Heterogeneity of Diagenesis and Reservoir Quality in Tight Sandstone: A Case Study from the Distributary Channel Belt in Shallow Water Delta of Triassic Yanchang Formation in Honghe Oilfield, Southern Ordos Basin. [Ph.D. thesis]. China University of Petroleum, Beijing.
- Li, S., Yu, X., Chen, B., Li, S., 2015. Quantitative characterization of architecture elements and their response to base-level change in a sandy braided fluvial system at a mountain front. *J. Sediment. Res.* 85, 1258–1274.
- Lunt, I.A., Bridge, J.S., Tye, R.S., 2004. A quantitative, three-dimensional depositional model of gravelly braided rivers. *Sedimentology* 51, 377–414.
- McBride, E.F., 1988. Contrasting diagenetic histories of concretions and host rock, Lion Mountain Sandstone (Cambrian). *Texas. Bull. Geol. Soc. Am.* 100, 1803–1810.
- McKinley, J.M., Atkinson, P.M., Lloyd, C.D., Ruffell, A.H., Worden, R.H., 2011. How porosity and permeability vary spatially with grain size, sorting, cement volume, and mineral dissolution in fluvial triassic sandstones: the value of geostatistics and local regression. *J. Sediment. Res.* 81, 844–858.
- Mohrig, D., Heller, P.L., Paola, C., Lyons, W.J., 2000. Interpreting avulsion process from ancient alluvial sequences: Guadalupe-Matarranya system (Northern Spain) and Wasatch Formation (Western Colorado). *Bull. Geol. Soc. Am.* 112, 1787–1803.
- Nichols, G.J., Fisher, J.A., 2007. Processes, facies and architecture of fluvial distributary system deposits. *Sediment. Geol.* 195, 75–90.
- Perrier, R., Jacques, Q., 1974. Thickness changes in sedimentary layers during compaction history; methods for quantitative evaluation. *Am. Assoc. Pet. Geol. Bull.* 58, 507–520.
- Schwartz, T.M., Fosdick, J.C., Graham, S.A., 2017. Using detrital zircon U-Pb ages to calculate Late Cretaceous sedimentation rates in the Magallanes-Austral basin. *Patagonia. Basin Res.* 29, 725–746.
- Slater, J.G., Christie, P.A.F., 1980. Continental stretching: an explanation of the post-mid-Cretaceous subsidence of the Central North Sea Basin. *J. Geophys. Res.* 85, 3711–3739.

- Screaton, E., Saffer, D., Henry, P., Hunze, S., 2002. Porosity loss within the underthrust sediments of the Nankai accretionary complex: implications for overpressures. *Geology* 30, 19–22.
- Wang, W., Yue, D., Zhao, J., Li, W., Wang, B., Wu, S., Li, S., 2019. Diagenetic alteration and its control on reservoir quality of tight sandstones in lacustrine deep-water gravity-flow deposits: a case study of the Yanchang Formation, southern Ordos Basin, China. *Mar. Pet. Geol.* 110, 676–694.
- Ward, N.I.P., Alves, T.M., Blenkinsop, T.G., 2018. Differential compaction over Late Miocene submarine channels in SE Brazil: implications for trap formation. *Bull. Geol. Soc. Am.* 130, 208–221.
- Wotherspoon, L.M., Pender, M.J., Orense, R.P., 2012. Relationship between observed liquefaction at Kaiapoi following the 2010 Darfield earthquake and former channels of the Waimakariri River. *Eng. Geol.* 125, 45–55.
- Xu, Q., Zhang, W., Pan, H., Wang, Y., Ying, C., Huang, Y., Pang, J., 2009. *Oil and Gas Industry Standards of China: Analysis Method for Particle Size of Clastic Rock* (No. SY/T 5434-2009). Petroleum Industry Press of China, Beijing.
- Yue, D., Li, W., Wang, W., Hu, G., Shen, B., Wang, W., Zhang, M., Hu, J., 2019. Analyzing the architecture of point bar of meandering fluvial river using ground penetration radar: a case study from Hulun Lake depression, China. *Interpretation* 7, 1–89.
- Zhang, C., Sun, W., Gao, H., 2014. Quantitative calculation of sandstone porosity evolution based on thin section data: a case study from Chang 8 reservoir of Huanjiang area, Ordos Basin (in Chinese). *Acta Sedimentol. Sin.* 32, 365–375.
- Zhu, R., Bai, B., Yuan, X., Luo, Z., 2013. A new approach for outcrop characterization and geostatistical analysis of meandering channels sandbodies within a delta plain setting using digital outcrop models: upper Triassic Yanchang tight sandstone Formation, Yanhe outcrop, Ordos Basin (in Chinese). *Acta Sedimentol. Sin.* 31, 867–877.
- Zhuo, H., Wang, Y., Shi, H., He, M., Chen, W., Li, H., Wang, Y., Yan, W., 2015. Contrasting fluvial styles across the mid-Pleistocene climate transition in the northern shelf of the South China Sea: evidence from 3D seismic data. *Quat. Sci. Rev.* 129, 128–146.